Mon. Not. R. Astron. Soc. **000**, 1–15 (2014) Printed 8 October 2013 (MN LATEX style file v2.2)

The Great Escape III: Placing post-main-sequence evolution of planetary and binary systems in a Galactic context

Dimitri Veras[1,2⋆], N. Wyn Evans[2], Mark C. Wyatt[2] and Christopher A. Tout[2]
[1] *Department of Physics, University of Warwick, Coventry CV4 7AL*
[2] *Institute of Astronomy, University of Cambridge, Cambridge CB3 0HA*

Accepted 2013 October 4. Received 2013 September 26; in original form 2013 July 23

ABSTRACT

Our improving understanding of the life cycle of planetary systems prompts investigations of the role of the Galactic environment before, during and after Asymptotic Giant Branch (AGB) stellar evolution. Here, we investigate the interplay between stellar mass loss, Galactic tidal perturbations, and stellar flybys for evolving stars which host one planet, smaller body or stellar binary companion and reside in the Milky Way's bulge or disc. We find that the potential evolutionary pathways from a main sequence (MS) to a white dwarf (WD) planetary system are a strong function of Galactocentric distance only with respect to the prevalence of stellar flybys. Planetary ejection and collision with the parent star should be more common towards the bulge. At a given location anywhere in the Galaxy, if the mass loss is adiabatic, then the secondary is likely to avoid close flybys during AGB evolution, and cannot eventually escape the resulting WD because of Galactic tides alone. Partly because AGB mass loss will shrink a planetary system's Hill ellipsoid axes by about 20 to 40 per cent, Oort clouds orbiting WDs are likely to be more depleted and dynamically excited than on the MS.

Key words: planets and satellites: dynamical evolution and stability – planet-star interactions – stars: AGB and post-AGB – stars: evolution – The Galaxy: kinematics and dynamics – Oort Cloud

1 INTRODUCTION

Planetary systems do not evolve in isolation. Their nascent orbital architectures may have been moulded by irradiation from, and the mutual interactions amongst, stars in a stellar birth cluster (Laughlin & Adams 1998; Bonnell et al. 2001; Smith & Bonnell 2001; Adams et al. 2006; Fregeau et al. 2006; Malmberg et al. 2007; Parker & Goodwin 2009; Spurzem et al. 2009; Thies et al. 2011; de Juan Ovelar et al. 2012; Parker & Quanz 2012; Marzari & Picogna 2013; Thompson 2013). Later, on the main sequence (MS), planetary orbits may be further disrupted by flybys from Galactic disc stars (Zakamska & Tremaine 2004; Malmberg et al. 2011; Boley et al. 2012; Veras & Moeckel 2012). The effect of flybys on debris discs and potential system habitability may be a strong function of Galactic environment (Jiménez-Torres et al. 2011, 2013). Gravitational scattering amongst multiple planets may be induced due to the effect of Galactic tides on wide binary stellar companions (Kaib et al. 2013). Oort clouds continuously interact with the Galactic environment; their content and extent are dictated by the combination of global Galactic tides as well as stellar flybys (Heisler & Tremaine 1986; Duncan et al. 1987; Dybczyński 2006; Emel'Yanenko et al. 2007; Rickman et al. 2008; Kaib & Quinn 2009; Brasser et al. 2010; Collins & Sari 2010; Brasser & Morbidelli 2013; Rickman 2013).

Modelling these effects during post-MS evolution provides new and largely unexplored challenges, and is the focus of this study. When stars evolve off the MS, they shed mass and expand their envelopes, occasionally out to several au. Planetary material too close to the star tidally interacts with the envelope (Soker 1998; Villaver & Livio 2007; Carlberg et al. 2009; Villaver & Livio 2009; Nordhaus et al. 2010; Kunitomo et al. 2011; Villaver 2011; Mustill & Villaver 2012; Passy et al. 2012; Spiegel 2012; Adams & Bloch 2013; Nordhaus & Spiegel 2013), with destruction being the likely, but not guaranteed, outcome (Maxted et al. 2006; Bear et al. 2011; Bear & Soker 2012).

A single orbiting body which survives giant branch evolution alters its orbit in a well-defined, analytically-precise manner in the isotropic mass loss limit (Omarov 1962; Hadjidemetriou 1963) as well as when the mass is lost anisotropically (Veras et al. 2013a). Detailed non-tidal studies of exoplanetary systems with stellar mass loss include post-MS explorations of

⋆ E-mail: d.veras@warwick.ac.uk

- 1-planet, 1-star systems: (Veras et al. 2011, hereinafter Paper I; Adams et al. 2013)
- 1-planet, 2-star systems: (Kratter & Perets 2012; Veras & Tout 2012, hereinafter Paper II)
- 2-planet, 1-star systems: (Debes & Sigurdsson 2002; Veras et al. 2013b; Voyatzis et al. 2013)
- 3-planet, 1-star systems: (Debes & Sigurdsson 2002; Mustill et al. 2013a)
- 2-planet, 2-star systems: (Portegies Zwart 2013; Mustill et al. 2013b)
- 0-planet, 1-star systems with a disc or cloud: (Parriott & Alcock 1998; Bonsor & Wyatt 2010)
- 1-planet, 1-star systems with a disc or cloud: (Bonsor et al. 2011; Debes et al. 2012)

Also, more generally, the restricted three-body problem with mass loss has been studied in a broad analytical context (e.g. Singh 2011; Varvoglis & Hadjidemetriou 2012; Zhang 2012).

Here, we compare the effects of mass loss, Galactic tides and stellar flybys for a single secondary body (e.g. planet, asteroid, comet or distant non-evolving star) orbiting a single primary star, and place these perturbations in the context of the entire lifetime of planetary systems, from the MS to the white dwarf (WD) phases. We consider a range of possible planetary separations, stellar separations from the Galactic centre, and WD progenitors. In Section 2, we describe our Galactic tidal model and present the equations of motion. Section 3 quantifies each effect and compares their strengths and reach. We give specific properties of the resulting orbital motion and outline potential evolutionary pathways in Section 4. Section 5 discusses implications and extensions, before we make our conclusions in Section 6.

2 GALACTIC MODEL

We consider a primary star of mass $M_\star$ that is orbiting the centre of the Milky Way Galaxy on a circular orbit in the Galactic plane. The secondary of mass $M_{\rm p}$ orbits the primary on an arbitrarily wide, elliptic and inclined orbit with respect to a reference plane that is parallel to and coincident with the Galactic plane. Both the primary and secondary are treated as point masses. The secondary may represent any non-evolving stellar companion; without loss of generality, we will often refer to it as a planet. This planetary system is orbiting the centre of Galaxy with circling frequency $\Omega_{\rm G}$ counterclockwise from the point of view of the North Galactic pole. The system is in the Galactic plane at a distance R from the Galactic centre. The star is undergoing post-main sequence evolution and is losing mass isotropically at the rate $\dot{M}_\star$; the isotropic mass loss approximation is robust for post-MS systems (Veras et al. 2013a).

2.1 Equations of motion

We adopt the same right-handed stellarcentric Cartesian coordinate system as Heisler & Tremaine (1986), Brasser et al. (2010), and Veras & Evans (2013a,b), with x pointing radially outwards, y pointing tangent to a star's motion in the Galactic disc and positive in the direction of Galactic rotation, and z pointing in the direction of the South Galactic Pole. The equations of motion for the planet are then

$$\frac{d^2x}{dt^2} = -\frac{G\left(M_\star(t)+M_{\rm p}\right)x}{\left(x^2+y^2+z^2\right)^{3/2}} + \Upsilon_{xx}x + \Upsilon_{xy}y, \quad (1)$$

$$\frac{d^2y}{dt^2} = -\frac{G\left(M_\star(t)+M_{\rm p}\right)y}{\left(x^2+y^2+z^2\right)^{3/2}} + \Upsilon_{yx}x + \Upsilon_{yy}y, \quad (2)$$

and

$$\frac{d^2z}{dt^2} = -\frac{G\left(M_\star(t)+M_{\rm p}\right)z}{\left(x^2+y^2+z^2\right)^{3/2}} + \Upsilon_{zz}z, \quad (3)$$

where the Υ terms are due to the Galactic tide. The perturbative acceleration due to isotropic mass loss is implicit – a phenomenon explained by Hadjidemetriou (1963) – and hence does not appear explicitly in equations (1)-(3). The following form of the Υ terms for circular stellar orbits in the Galactic disc around the Galactic centre are derived by Brasser et al. (2010) and Veras & Evans (2013b):

$$\Upsilon_{xx} = {\Omega_{\rm G}}^2[(1-\delta)\cos\left(2\Omega_{\rm G}t\right)-\delta], \quad (4)$$

$$\Upsilon_{xy} = {\Omega_{\rm G}}^2(1-\delta)\sin\left(2\Omega_{\rm G}t\right), \quad (5)$$

$$\Upsilon_{yx} = {\Omega_{\rm G}}^2(1-\delta)\sin\left(2\Omega_{\rm G}t\right), \quad (6)$$

$$\Upsilon_{yy} = -{\Omega_{\rm G}}^2[(1-\delta)\cos\left(2\Omega_{\rm G}t\right)+\delta], \quad (7)$$

and

$$\Upsilon_{zz} = -\left[4\pi G\rho_{\rm tot} - 2\delta{\Omega_{\rm G}}^2\right], \quad (8)$$

where $\delta \equiv -(A+B)/(A-B)$ represents the logarithmic gradient of the Galactic rotation curve in terms of the Oort Constants A and B (Matese & Whitmire 1996). The expressions for $\Omega_{\rm G}$, A and B are obtained from the three-component Galaxy model presented by Veras & Evans (2013b), and the total Galactic density $\rho_{\rm tot}$ is described below.

2.2 Matter density

The total density of the Galaxy, including both stars and dark matter, is denoted by $\rho_{\rm tot}(R,z)$ in terms of cylindrical polar coordinates (R,z). This density is composed of an exponential disc, a Hernquist bulge and a cored isothermal halo that together reproduce the local stellar kinematics.

The stellar bulge has a Hernquist profile with mass $M_{\rm b}$ and scalelength a_h:

$$\rho_{\rm bulge}(R,z) = \frac{a_h M_{\rm b}}{2\pi\sqrt{R^2+z^2}\left(\sqrt{R^2+z^2}+a_h\right)^3}, \quad (9)$$

The stellar disc is a double exponential with scalelength $R_{\rm d}$ and scaleheight h:

$$\rho_{\rm disc}(R,z) = \frac{\Sigma_0}{2h}\exp\left(-\frac{R}{R_{\rm d}}\right)\exp\left(-\frac{|z|}{h}\right), \quad (10)$$

The dark matter halo is a cored, isothermal model with core radius $R_{\rm c}$ and asymptotic amplitude of rotation curve v_0 (Evans 1993):

$$\rho_{\rm halo}(R,z) = \frac{v_0^2}{4\pi G q^2}\frac{{R_{\rm c}}^2\left(1+2q^2\right)+R^2+z^2(2-q^{-2})}{{R_{\rm c}}^2+R^2+z^2q^{-2}}. \quad (11)$$

We adopt the same numerical values as Veras & Evans (2013b) for the bulge mass, $M_{\rm b} = 3.6\times10^{10}M_\odot$, Hernquist potential parameter $a_h = 0.7$ kpc, thin disc scale height $h = 0.3$ kpc, thin disc scale length $R_{\rm d} = 3$ kpc, circular velocity $v_0 = 215$ km s^{-1}, core radius $R_{\rm c} = 16$ kpc, normalisation surface density

constant $\Sigma_0 = 51 \times \exp(8\ \mathrm{kpc}/R_\mathrm{d}) M_\odot \mathrm{pc}^{-2}$ and equipotential axis ratio $q = 1$. Adopting these values for our model allows us to closely reproduce observations of all the local stellar kinematics, as described in Veras & Evans (2013b).

The Galaxy model that we use reproduces the local stellar kinematics. It has of course some arbitrariness, as the three-dimensional density distributions of the bulge and halo are not well known. For example, cusped Navarro-Frenk-White (NFW) models are often used for halos, motivated by dissipationless cosmological simulations. They differ from cored isothermal halos, particularly at the centre. However, when baryonic effects are included in galaxy formation simulations, they transfer energy between the luminous and dark components, producing a shallower or cored profile for the dark matter. This is consistent with observational data on the Galaxy, which precludes strongly cuspy halos (like the NFW) using constraints from the rotation curve and the microlensing experiments (Binney & Evans 2001). Similarly, there are a number of possible models for the Galactic bulge, depending on whether its origin is through mergers or through secular disk processes or though thickening of a Galactic bar (Kormendy & Kennicutt 2004). We have used a Hernquist model, but exponential or Sersic models could easily have been used instead. The main advantage of a Hernquist model is that the gravitational force-field is analytic, which speeds numerical orbit integrations. Sersic models in general do not have analytic potentials.

2.3 Frequencies and velocities

The circular frequency in the Galactic plane is given by

$$\Omega_\mathrm{G}{}^2(R) = \underbrace{\frac{GM_b}{R\left(R+a_h\right)^2}}_{\text{bulge}} + \underbrace{\frac{v_0^2}{R_\mathrm{c}{}^2+R^2}}_{\text{halo}} + \underbrace{\frac{G\pi\Sigma_0}{R_\mathrm{d}}\left[I_0\left(\frac{R}{2R_\mathrm{d}}\right)K_0\left(\frac{R}{2R_\mathrm{d}}\right) - I_1\left(\frac{R}{2R_\mathrm{d}}\right)K_1\left(\frac{R}{2R_\mathrm{d}}\right)\right]}_{\text{disc}}, \quad (12)$$

where I_0, I_1, K_0 and K_1 are modified Bessel functions. The circular velocity $v_\mathrm{c} = R\Omega_\mathrm{G}$. The Oort constants are

$$A = \frac{1}{2}\left[\Omega_\mathrm{G} - \frac{dv_\mathrm{c}}{dR}\right], \qquad \text{and} \qquad B = -\frac{1}{2}\left[\Omega_\mathrm{G} + \frac{dv_\mathrm{c}}{dR}\right], \quad (13)$$

with

$$\frac{dv_\mathrm{c}}{dR} = \underbrace{\frac{GM_\mathrm{b}\left(a_h - R\right)}{2\Omega_\mathrm{G} R\left(R+a_h\right)^3}}_{\text{bulge}} + \underbrace{\frac{R_\mathrm{c}{}^2 v_0^2}{\Omega_\mathrm{G}\left(R_\mathrm{c}{}^2+R^2\right)^2}}_{\text{halo}} + \frac{G\pi\Sigma_0}{2\Omega_\mathrm{G} R_\mathrm{d}{}^2}\left\{RI_1\left(\frac{R}{2R_\mathrm{d}}\right)K_0\left(\frac{R}{2R_\mathrm{d}}\right) + I_0\left(\frac{R}{2R_\mathrm{d}}\right)\left[2R_\mathrm{d}K_0\left(\frac{R}{2R_\mathrm{d}}\right) - RK_1\left(\frac{R}{2R_\mathrm{d}}\right)\right]\right\}. \quad (14)$$

The last term is the contribution from the Galactic disc. This term has been simplified by exploiting the relationships between Bessel functions of different orders.

2.4 Re-expressed perturbative accelerations

Equations (9)-(14) allow us to re-express the form of the perturbations in equations (4)-(8) and eliminate δ. Doing so will aid further analysis. First, note that $\Omega_\mathrm{G}\delta = dv_\mathrm{c}/dR$ and $(1-\delta)\,\Omega_\mathrm{G} = \Omega_\mathrm{G} - dv_\mathrm{c}/dR$. Consequently, equations (4)-(8) can be rewritten as

$$\Upsilon_{xx} = -\Omega_\mathrm{G}\frac{dv_\mathrm{c}}{dR} - \left(\Omega_\mathrm{G}{}^2 - \Omega_\mathrm{G}\frac{dv_\mathrm{c}}{dR}\right)\cos\left(2\Omega_\mathrm{G}t\right), \quad (15)$$

$$\Upsilon_{yy} = -\Omega_\mathrm{G}\frac{dv_\mathrm{c}}{dR} + \left(\Omega_\mathrm{G}{}^2 - \Omega_\mathrm{G}\frac{dv_\mathrm{c}}{dR}\right)\cos\left(2\Omega_\mathrm{G}t\right), \quad (16)$$

$$\Upsilon_{xy} = \Upsilon_{yx} = -\left(\Omega_\mathrm{G}{}^2 - \Omega_\mathrm{G}\frac{dv_\mathrm{c}}{dR}\right)\sin\left(2\Omega_G t\right) \quad (17)$$

and

$$\Upsilon_{zz} = -\left[4\pi G\rho_G - 2\Omega_\mathrm{G}\frac{dv_\mathrm{c}}{dR}\right] = -\Omega_\mathrm{G}{}^2|_\mathrm{bulge} - \Omega_\mathrm{G}{}^2|_\mathrm{halo} - G\pi\Sigma_0\left[\frac{2}{h}\exp\left(-\frac{R}{R_\mathrm{d}}\right) - \frac{1}{R_\mathrm{d}{}^2}\left\{RI_1\left(\frac{R}{2R_\mathrm{d}}\right)K_0\left(\frac{R}{2R_\mathrm{d}}\right) + I_0\left(\frac{R}{2R_\mathrm{d}}\right)\left[2R_\mathrm{d}K_0\left(\frac{R}{2R_\mathrm{d}}\right) - RK_1\left(\frac{R}{2R_\mathrm{d}}\right)\right]\right\}\right], \quad (18)$$

where the last vertical perturbative term is the contribution from the disc. We will later show that the quantity in parenthesis for the planar cross-term (in equation 17) scales with the region of gravitational influence of an individual star. Also, note that the bulge and halo components of equation (18) reduce exactly to the corresponding components of equation (12).

3 COMPARISON OF EFFECTS

Having presented our Galactic model, we now characterize the regimes in which different effects may be important by comparing the timescales for orbital motion, mass loss, and Galactic tides. We then place impulsive stellar encounters in this picture. We conclude with plots that combine all these effects.

3.1 Post-MS timescale

We define two nondimensional indices. The first is from Paper I:

$$\Psi_\mathrm{PMS}(t) \equiv \frac{\text{orbital timescale}}{\text{mass}-\text{loss timescale}} = \frac{\dot{\mu}(t)}{n(t)\mu(t)}$$

$$\approx 0.16\left(\frac{\dot{M}_\star(t)}{1M_\odot \mathrm{yr}^{-1}}\right)\left(\frac{a(t)}{1\mathrm{AU}}\right)^{\frac{3}{2}}\left(\frac{M_\star(t)+M_\mathrm{p}}{1M_\odot}\right)^{-\frac{3}{2}}, \quad (19)$$

where a represents the planet's semimajor axis, n the planet's mean motion and $\mu = G\left(M_\star + M_\mathrm{p}\right)$.

The index Ψ_PMS provides a measure of the mass-loss adiabaticity of a system. In a system which is adiabatic with respect to mass loss, the semimajor axis increases at a steady rate and the eccentricity remains unchanged[1]. In a nonadiabatic system,

[1] There is a typographic error in equation (17) of Paper I; the denominator should read $1 + e_0\cos f$ (G. Voyatzis, priv. comm).

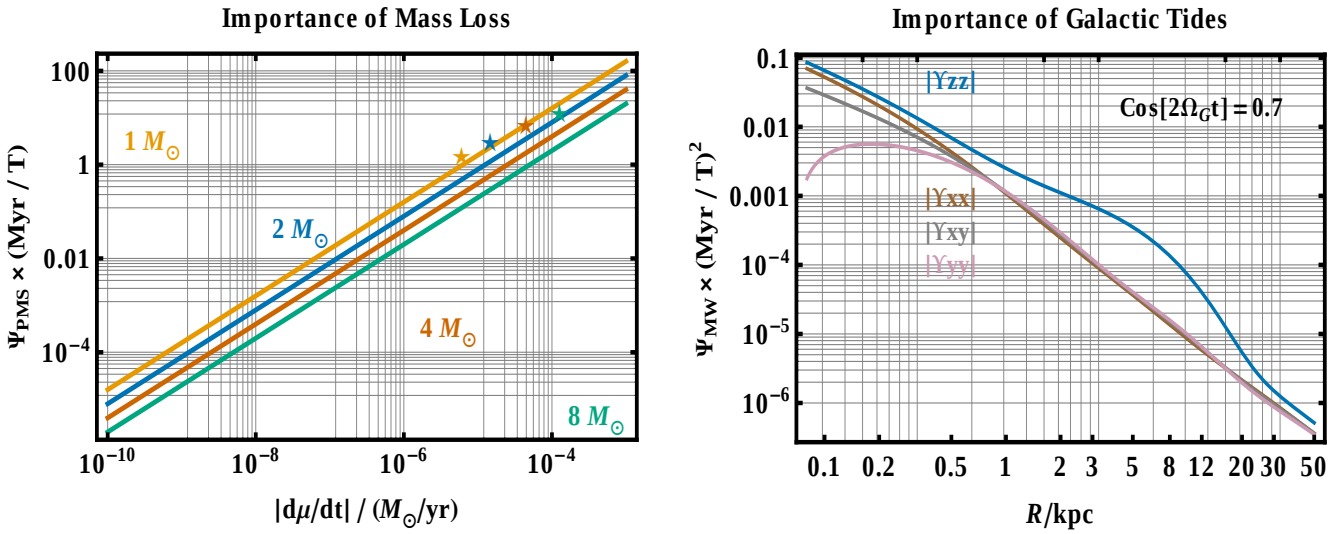

Figure 1. A demonstration that orbital effects due to post-MS mass loss may be decoupled from the effects due to Galactic tides. The dimensionless adiabaticity indices ($\Psi_{\rm PMS}, \Psi_{\rm MW}$) for stellar mass loss (*left panel*) and for a snapshot of Galactic tides (*right panel*) represent how actively a secondary's orbit is influenced by these effects. Nonadiabatic influences typically become important when $\Psi \gtrsim 0.02$. T represents the orbital period of the secondary, and five-pointed stars indicate the highest $\Psi_{\rm PMS}$ reached in stellar evolution models. Although the Galactic tide adiabaticity index is a function of time, the maximum perturbation is well-represented by the topmost curve for all times and Galactocentric distances.

the eccentricity can change and trigger instability. The transition is not sharp; substantial deviations from adiabaticity can occur at $\Psi_{\rm PMS} \approx 0.02$ (see e.g. fig. 3 of Paper I).

In Fig. 1, we plot $\Psi_{\rm PMS}$ as a function of mass-loss rate for four different stellar masses. $\Psi_{\rm PMS}$ is scaled by the secondary orbital period T. The coloured stars indicate the highest $\Psi_{\rm PMS}$ values achieved during simulations of stellar evolutionary models with the `SSE` code (Hurley et al. 2000). The `SSE` code uses a Reimers mass loss prescription with a coefficient of 0.5 on the Red Giant Branch (RGB) and the mass loss prescription from Vassiliadis & Wood (1993) on the Asymptotic Giant Branch (AGB). The stars in the figure do not lie on the lines because the highest value of $\Psi_{\rm PMS}$ is achieved in each case after the star has lost some of its original mass. The highest values of $\Psi_{\rm PMS}$ achieved in the simulations correlates closely to the highest values of mass loss experienced by the parent stars. The figure demonstrates, for example, that a planet orbiting a $1M_\star$ star at $a = 10^4$ au experiences nonadiabatic evolution if the parent star loses mass at a rate greater than about $10^{-7} M_\odot$ yr^{-1}. As the position of the yellow star suggests, this mass-loss rate is thought to be easily achieved by AGB stars.

3.2 Galactic tidal timescale

We define the Galactic tidal timescale index as:

$$\Psi_{\rm MW}(t) \equiv \frac{\text{orbital timescale}}{\text{Galactic tidal timescale}} \approx \frac{\Upsilon(t)}{n(t)^2}. \qquad (20)$$

This index provides a measure of the Galactic tidal adiabaticity of a system. The orbital properties of adiabatic systems measured with respect to Galactic tides are different than those measured with respect to mass loss, and will be described later in Sections 4.1-4.2. The time dependence of Υ arises from the planar tidal terms only. However, as we will show $\max|\Upsilon| = |\Upsilon_{zz}|$ everywhere except within the inner 500 pc area of the Milky Way. Further, in this inner bulge region, $|\Upsilon_{zz}|$ is comparable to the maximum planar perturbation. Hence, we approximate $|\Upsilon|$ by $|\Upsilon_{zz}|$ only.

In the right panel of Fig. 1, we plot $|\Upsilon_{zz}|$, as well as a snapshot of $|\Upsilon_{xx}|$ and $|\Upsilon_{xy}|$, which are time-dependent. The approximate maximum value of $|\Upsilon|$ for all times and Galactocentric distances is the topmost curve. The plot demonstrates that the prospects for a companion to undergo nonadiabatic evolution due to Galactic tides is a strong function of both Galactic position and orbital period. Assuming an adiabatic limit of $\Psi_{\rm MW} \approx 0.02$, a planet with a period of 1 Myr (corresponding to $a = 10^4$ AU around a $1M_\odot$ star) is affected by tides adiabatically throughout the Milky Way except within the first few hundred parsecs. However, increasing this semimajor axis by a factor of 5 lowers the adiabaticity boundary by a factor of 125, causing any planet within the Solar circle ($R \lesssim 8$ kpc) to undergo nonadiabatic evolution due to Galactic tides.

3.3 Timescale comparison

Comparing both plots in Fig. 1 side-by-side helps us to establish the expected level of coupling between mass loss and Galactic tides with respect to orbital excitation. For a given planetary orbital period (fixed T), and for any parent star experiencing post-MS evolution, $\Psi_{\rm PMS} \gtrsim \Psi_{\rm MW}$ holds true, and often $\Psi_{\rm PMS} \gg \Psi_{\rm MW}$ is satisfied. Hence, the effects of post-MS mass loss and Galactic tides can effectively be decoupled when the former is active.

3.4 The Hill ellipsoid

If the secondary is sufficiently far from the primary, then the secondary will escape. Veras & Evans (2013b) showed that the Hill sphere in this instance is actually a triaxial ellipsoid with extent

$$\vec{r}_{\rm Hill} = \left(\frac{GM_\star}{\alpha}\right)^{1/3} \vec{k} \tag{21}$$

such that

$$\vec{k} = \left(1, \frac{2}{3}, \frac{\left[Q\left(1+\sqrt{1+Q}\right)\right]^{2/3} - Q}{\left[Q\left(1+\sqrt{1+Q}\right)\right]^{1/3}}\right), \tag{22}$$

where $Q \equiv -\alpha/\Upsilon_{zz}$ and[2] $\alpha \equiv 4A\,(A-B)$. The third (z) component of $\vec{k}$ lies in the range $(0, 2/3)$. Simplification shows that $\alpha = 2\left[{\Omega_{\rm G}}^2 - \Omega_{\rm G}\,(dv_{\rm c}/dR)\right]$, meaning that the perturbations of equations (15-17) can be expressed simply in terms of the Hill ellipsoid axes through $\Upsilon_{xx} = -{\Omega_{\rm G}}^2 + (\alpha/2)[1-\cos(2\Omega_{\rm G}t)]$, $\Upsilon_{yy} = -{\Omega_{\rm G}}^2 + (\alpha/2)[1+\cos(2\Omega_{\rm G}t)]$ and $\Upsilon_{xy} = \Upsilon_{yx} = -2\alpha\sin(2\Omega_{\rm G}t)$. Therefore, expressed in Hill radii, planar perturbation maxima are

$$|\Upsilon_{xy}|_{\rm max} = \frac{2GM_\star}{r^3_{{\rm Hill},x}} \tag{23}$$

and

$$|\Upsilon_{xx}|_{\rm max} = |\Upsilon_{yy}|_{\rm max} = \frac{GM_\star}{r^3_{{\rm Hill},x}} - {\Omega_{\rm G}}^2. \tag{24}$$

Having defined the Hill ellipsoid and related it to the magnitude of the perturbations, we can now assess the adiabaticity of orbits at the Hill limit. Using equation (21), we find that the slowest possible mean motion of a companion is

$$n_{\rm min} = \left[\frac{1-e^2}{1+e\cos f}\right]^{\frac{3}{2}} \sqrt{\left|\frac{\alpha}{k_z^3}\right|} < \frac{3}{2}\sqrt{\frac{3\alpha}{2}}\,(1+e)^{\frac{3}{2}}\,, \tag{25}$$

where e is eccentricity and f is the true anomaly. Further, in the limit of small Q and for circular orbits, $n_{\rm min} \approx \sqrt{\Upsilon_{zz}/2}$. Hence, we can combine this relation with equation (20) in order to relate the minimum Hill semiaxis (z) with the adiabatic Galactic tidal limit. Doing so gives $T_{\rm Hill}/T_{\rm Gal} \approx \sqrt{2/\Psi_{\rm MW}}$, independent of R, where $T_{\rm Hill}$ and $T_{\rm Gal}$ represent the orbital periods at the Hill limit and the nonadiabatic Galactic limit. Therefore, Galactic effects become non-adiabatic at a nearly fixed fraction of the Hill limit, and orbits at the Hill limit are always non-adiabatic.

3.5 Stellar flybys

A final consideration is the effect of stellar flybys on planetary systems. This type of perturbation is a scaled-down version of the well-studied and more general scenario of stars flying past binary stellar systems (Chapters 6,8,10 of Valtonen & Karttunen 2006). The seminal work of Heggie (1975) helped lay the analytical framework for modeling this dynamical three-body interaction. Early numerical integration ensembles (Hills & Fullerton 1980; Hills 1984a) provided further insight that is sometimes difficult to parse from the analytics. Subsequent investigations focusing on the Solar System (e.g. Hills 1984b, 1986) linked flybys with the Oort cloud, and others studies considered repeated flybys in different astrophysical contexts. Hills (1984c), for example, found that binaries in globular clusters are more resistant to changes in semimajor axis than eccentricity.

Such orbital element variation tendencies will have important consequences for detailed studies of repeated flybys on planetary systems. Heggie & Rasio (1996) significantly facilitated understanding of how orbits change due to flybys by deriving explicit analytic formulas in terms of orbital elements due to slow and distant encounters. Although application of these formulae exceeds the scope of this study, alternatively we consider flybys in the impulsive limit. A.P. Jackson et al. (2013, In Prep) provide a comprehensive and fully general set of orbital element changes due to impulses. Here, however, we use simple approximations (Veras & Moeckel 2012) and escape criteria to bound the effects.

[2] There is a sign error in the definitions of α and Q in Veras & Evans (2013b).

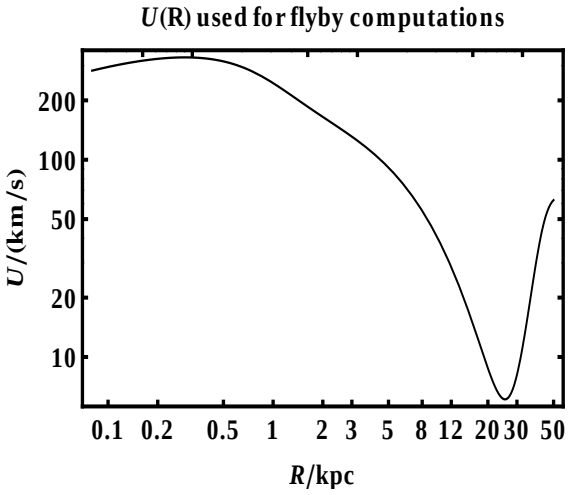

Figure 2. Flyby velocity profile throughout the Milky Way for a host star on a circular orbit in the Galactic disc (equation 31).

3.5.1 Impact parameter

Within a timescale Δt, the closest expected encounter distance, or impact parameter b, is (see e.g. Binney & Tremaine 2008)

$$b(R) \approx \left[4\pi\left(\frac{\rho_{\rm stars}(R)}{\langle M_{\rm stars}\rangle}\right) U(R)\Delta t\right]^{-1/2}, \tag{26}$$

where the quantity in the large parenthesis is the stellar number density. Here, U is the relative velocity of the stars at an infinite separation, and $\langle M_{\rm stars}\rangle$ is the average stellar mass. In our calculations, we assume that in the bulge and disc, all of the mass is in stars, whereas in the halo, all of the mass is in dark matter. We take $\langle M_{\rm stars}\rangle = 0.88 M_\odot$ (Parravano et al. 2011).

3.5.2 Flyby velocity

We can obtain a prescription for $U(R)$ by considering the bulge and disc flyby stars separately. We approximate $U(R)$ by the average relative velocity of the flyby stars to the host, so that $U(R) = \left\langle (V_{\rm star} - V_{\rm fl})^2 \right\rangle^{1/2}$, where $V_{\rm fl}$ is the velocity of the flyby star. The value of $U(R)$ depends on position, as the velocities of bulge and disk stars vary within the Galaxy.

The host stars are on circular orbits about the Galactic centre. Therefore, their motion is in the azimuthal (ϕ) direction only with a speed given by the magnitude of the circular velocity $v_{\rm c}$. Now, let us consider the disk and bulge populations providing the flybys. The velocity dispersion components of the (non-rotating) Hernquist (1990) bulge are

$$\left\langle V^2_{R,{\rm bulge}}\right\rangle = \left\langle V^2_{\theta,{\rm bulge}}\right\rangle = \left\langle V^2_{\phi,{\rm bulge}}\right\rangle$$

$$= \frac{GM_b}{12a_h}\left[\left(\frac{12R\left(R+a_h\right)^3}{{a_h}^4}\right)\ln\left(\frac{R+a_h}{R}\right)\right.$$

$$\left.-\left(\frac{R}{R+a_h}\right)\left(25+52\frac{R}{a_h}+42\frac{R^2}{{a_h}^2}+12\frac{R^3}{{a_h}^3}\right)\right]. \quad (27)$$

This model serves for first calculations of the effect of flybys even though the Milky Way bulge is triaxial and rotating.

For the disc stars, the velocity dispersion around the circular speed is taken as (see e.g. Evans & Collett 1993; Bottema 1993; van der Kruit & Freeman 2011)

$$\left\langle V_{R,\rm disc}^2\right\rangle = \frac{\left\langle V_{z,\rm disc}^2\right\rangle}{\exp\left(1\right)} = 2\left\langle V_{\phi,\rm disc}^2\right\rangle = \sigma_0^2\exp\left(-\frac{R}{R_{\rm d}}\right), \quad (28)$$

with $\sigma_0 = 100$ km s^{-1}. Here, we have used epicylic theory to relate the radial and azimuthal dispersions, and the empirical equation (11) of van der Kruit & Freeman (2011) to relate the radial and vertical dispersions.

Therefore, the square of the average relative velocity of flybys in each Galactic component is

$$U_{\rm bulge}^2 = \left\langle V_{R,\rm bulge}^2\right\rangle + \left\langle V_{\theta,\rm bulge}^2\right\rangle + \left\langle\left(v_{\rm c}-V_{\phi,\rm bulge}\right)^2\right\rangle$$
$$= \left\langle V_{R,\rm bulge}^2\right\rangle + \left\langle V_{\theta,\rm bulge}^2\right\rangle + \left\langle V_{\phi,\rm bulge}^2\right\rangle + v_{\rm c}^2 \quad (29)$$

and

$$U_{\rm disc}^2 = \left\langle V_{R,\rm disc}^2\right\rangle + \left\langle\left(v_{\rm c}-\left(v_{\rm c}+V_{\phi,\rm disc}\right)\right)^2\right\rangle + \left\langle V_{z,\rm disc}^2\right\rangle$$
$$= \left\langle V_{R,\rm disc}^2\right\rangle + \left\langle V_{z,\rm disc}^2\right\rangle + \left\langle V_{\phi,\rm disc}^2\right\rangle. \quad (30)$$

Here, we have neglected the asymmetric drift and assumed that the stellar disk rotational velocity is v_c. We now weight the contributions from bulge and disc proportionally so that

$$U(R) = U_{\rm bulge}\frac{\rho_{\rm bulge}}{\rho_{\rm disc}+\rho_{\rm bulge}} + U_{\rm disc}\frac{\rho_{\rm disc}}{\rho_{\rm disc}+\rho_{\rm bulge}}. \quad (31)$$

In Fig. 2 we plot the $U(R)$ profile throughout the Milky Way. Although it has been derived with a number of approximations and simplifications, the profile is a useful guide to the average relative velocity of flybys in the Galaxy.

3.5.3 Kick velocity

The relation between a resulting kick velocity Δv on a planet due to the flyby velocity U is a function of the orientation of the encounter. We can evaluate the possible range of Δv by considering the extreme cases presented by Veras & Moeckel (2012). Let the mass of the flyby star be $M_{\rm fl}$. The minimum and maximum Δv are given by

$$\Delta v = \frac{2bU^3}{G\left(M_{\rm fl}+M_\star\right)}\left(1+\frac{b^2U^4}{G^2\left(M_{\rm fl}+M_\star\right)^2}\right)^{-2}$$
$$-\frac{2b'U^3}{G\left(M_{\rm fl}+M_{\rm p}\right)}\left(1+\frac{b'^2U^4}{G^2\left(M_{\rm fl}+M_{\rm p}\right)^2}\right)^{-1}, \quad (32)$$

where

$$b' = \left(u\pm a\right)\frac{bU^2}{G\left(M_{\rm fl}+M_\star\right)}\left(1+\frac{b^2U^4}{G^2\left(M_{\rm fl}+M_{\rm p}\right)^2}\right)^{-\frac{1}{2}} \quad (33)$$

and

$$u = \frac{G\left(M_{\rm fl}+M_\star\right)}{U^2}\left[\sqrt{1+\frac{b^2U^4}{G^2\left(M_{\rm fl}+M_\star\right)^2}}-1\right] \quad (34)$$

corresponding to coplanar encounters on the opposite or same side from the planet.

3.5.4 Criteria for impulse, escape & boundedness

In order for the impulse approximation to be applicable, the ratio of the orbital period of the planet to the encounter timescale must be much greater than unity. Hence, if we assume the closest impact parameter is equivalent to a, then the criterion is equivalent to

$$10\left(\frac{T}{10^5{\rm yr}}\right)^{\frac{1}{3}}\left(\frac{U}{1{\rm km\ s^{-1}}}\right)\left(\frac{M_\star+M_{\rm p}}{M_\odot}\right)^{-\frac{1}{3}} \gg 1. \quad (35)$$

Given that generally $U \gtrsim 10$ km s^{-1} outside of stellar clusters throughout the Milky Way's bulge and disc, the impulse approximation should easily be applicable for orbital periods greater than tens of years.

This approximation allows us to bound the motion of the secondary. The absolute minimum value of Δv for which a planet may escape is $\Delta v_{\rm min} = \left(\sqrt{2}-1\right)\sqrt{G\left(M_\star+M_{\rm p}\right)/a}$. Similarly the absolute maximum value of Δv for which a planet is guaranteed to remain bound is $\Delta v_{\rm max} = \left(\sqrt{2}+1\right)\sqrt{G\left(M_\star+M_{\rm p}\right)/a}$. With these criteria[3] and equations (32)-(34), we find that planets may either be guaranteed to escape or guaranteed to remain bound depending entirely on the orientation of the collision. For example, a $M_{\rm p} = 0.001M_\odot$ planet (like Jupiter) in a circular orbit around a $1M_\odot$ star at 1000 au that is perturbed by another $1M_\odot$ star with $U = 100$ km s^{-1} and $b = 1000$ au endures a Δv that is anywhere between about 0.027 km s^{-1} and 80.09 km s^{-1}, whereas $\Delta v_{\rm min} = 0.39$ km s^{-1} and $\Delta v_{\rm max} = 2.28$ km s^{-1}. A decrease in U by a factor of 10 reduces the range of Δv by about just an order of magnitude. This range still encompasses $\Delta v_{\rm min}$ and $\Delta v_{\rm max}$.

Unfortunately then, we cannot place restrictions on how planets would be perturbed by flybys without performing a much more detailed study. In the absence of a more concrete measure, we can relate the closest expected encounter distance over a given timescale (equation 26) with the semimajor axis of the secondary's orbit. By equating these two quantities, we obtain a critical semimajor axis, or orbital period, which will be used in the next section to compare with the effects from mass loss and Galactic tides. Exploring the quality of this metric, especially compared to the effects from multiple much more distant stellar encounters, is a subject for future studies.

3.6 Summary plots

We now combine equations (19), (20), (25) and (26) in Fig. 3, which is the main result of this paper. The plots describe different regimes of motion due to various effects for a single planet, brown dwarf or other companion to an evolving primary star.

The value of Ψ, assumed here to be equal to both $\Psi_{\rm PMS}$ and $\Psi_{\rm MW}$, indicates the extent of adiabaticity prescribed. For example, comets with $e \approx 0.99$ need just a slight nudge to prompt escape or collision, so that in this case one should consider a value of Ψ lower than 0.02.

The horizontal black lines indicate the adiabatic mass-loss

[3] See A.P. Jackson et al. (2013, In Prep) for additional information about the effect of Δv kicks on orbital motion.

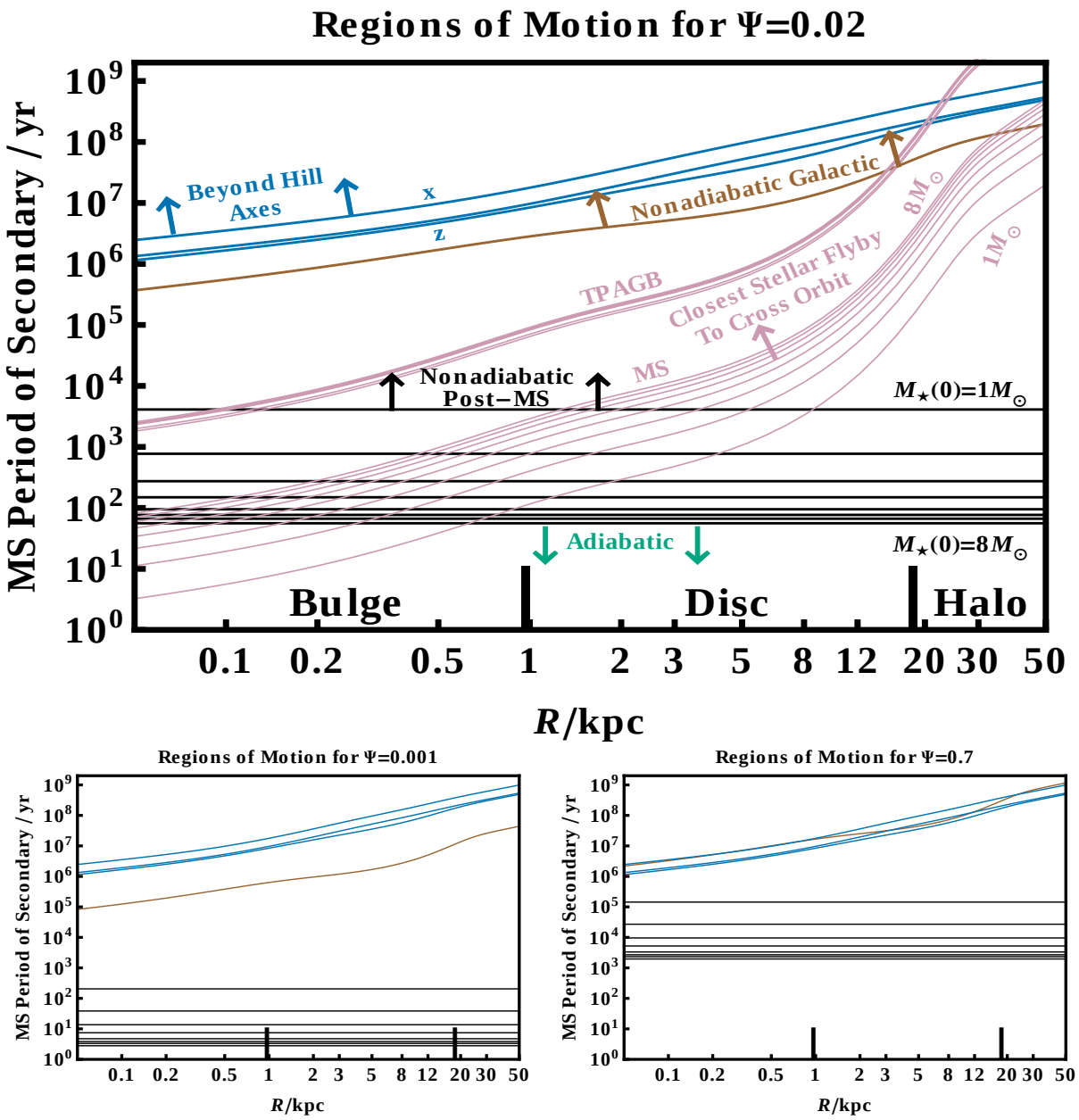

Figure 3. Regions where MS planets are under the influence of post-MS stellar mass loss, Galactic tides and stellar flybys. The strength of these first two effects are measured by the nondimensional indices $\Psi_{\rm PMS}$ and $\Psi_{\rm MW}$, which are both set equal to Ψ here. When Ψ exceeds values such as 0.001, 0.02 and 0.7, then the system becomes nonadiabiatic to different extents. The standard value is approximately 0.02. Adiabatic stellar mass loss increases a but leaves e fixed, whereas adiabatic Galactic tides changes e but leave a fixed. Neither variable is fixed in the nonadiabatic cases. Close stellar flybys may or may not occur; if they do, then their influence is strongly dependent on the orientation of the encounter. See Section 3.5 for a detailed description of this figure.

boundary for stars of progenitor masses of $1M_{\odot}$, $2M_{\odot}$, $3M_{\odot}$, $4M_{\odot}$, $5M_{\odot}$, $6M_{\odot}$, $7M_{\odot}$ and $8M_{\odot}$. We compute this boundary by identifying the critical time $t_{\rm crit}$ at which $\max[\Psi_{\rm PMS}(t)]$ equals 0.02, 0.7 and 0.001 (per each figure in the plot). We then derived the planet's period from $a(t_{\rm crit})$ in equation (19). All of the stellar evolutionary tracks were computed with `SSE`.

The Galactic adiabaticity boundary (brown line) is computed with $\Psi_{\rm MW}$ and $|\Upsilon_{zz}|$, as justified previously. Note importantly that the post-MS adiabaticity boundary is lower than the Galactic adiabaticity boundary by at least an order of magnitude always and everywhere except perhaps within a few parsecs of the Galactic centre or for stars with masses much lower than $1M_{\odot}$. Because any star which becomes a WD can lose at most about 80 per cent of its mass, a planet's semimajor axis can expand adiabatically by at most a factor of about 5. Hence adiabatic mass loss cannot alone expand an orbit into the nonadiabatic Galactic region.

The region in which nonadiabatic Galactic tides act is small (about a decade in planetary period) because the Galactic adiabaticity boundary coincides with the Hill ellipsoid (blue line) for $\Psi_{\rm MW} \approx 2$ (see Section 3.3). A planet beyond the Hill ellipsoid escapes the system. The blue lines remain unchanged during the

WD phase, despite the shrinkage of the Hill axis (equation 21) from AGB mass loss because the orbital period is increased by the same factor.

The pink lines in Fig. 3 indicate the limit for close encounters to occur at the radius of the planet's orbit. The lines were computed using equation (26) with Δt representing the Thermally Pulsing Asymptotic Giant Branch (TPAGB) lifetime for the top set of lines and the MS lifetime for the bottom set of lines. The thermally pulsing phase occurs near the end of giant branch evolution, when the greatest amount of mass is lost at the greatest rate. Any planets residing below the top pink lines should remain undisturbed by close stellar flybys during TPAGB evolution. Planets evolving adiabatically due to mass loss are generally protected from flybys. The lower set of pink lines indicates that close flybys may be a common, endemic feature of MS evolution. The flybys could play a similarly important role during WD evolution.

We can garner intuition for Fig. 3 as well as help to affirm its usefulness in characterizing individual exosystems by considering the Solar System. Figure 4 displays a vertical slice of Fig. 3 at $R = 8$ kpc, with $M_\star = 1M_\odot$ along the MS. All three Hill semiaxes are plotted, as well as the three non-adiabatic boundaries for mass loss and Galactic tides for $\Psi = \{0.001, 0.02, 0.7\}$. Additionally, the pink line corresponding to the limit for close encounters to occur is plotted, and lies at about 222 au from the Sun. This value correlates well with the 500 au, 5 Gyr Solar neighbourhood estimate of Zakamska & Tremaine (2004) and the couple hundred au, full MS lifetime estimates of Veras & Moeckel (2012). Also, the non-adiabatic mass loss limit for $\Psi = 0.7$, at about 2740 au, lies within the Solar System's post-MS escape boundary range of $10^3 - 10^4$ au assuming $\Psi = 1.0$ (Veras & Wyatt 2012). The implication for exosystems like our Solar System is that most secondaries which will experience any type of non-adiabatic motion will probably also have their orbits crossed at least once by a passing star.

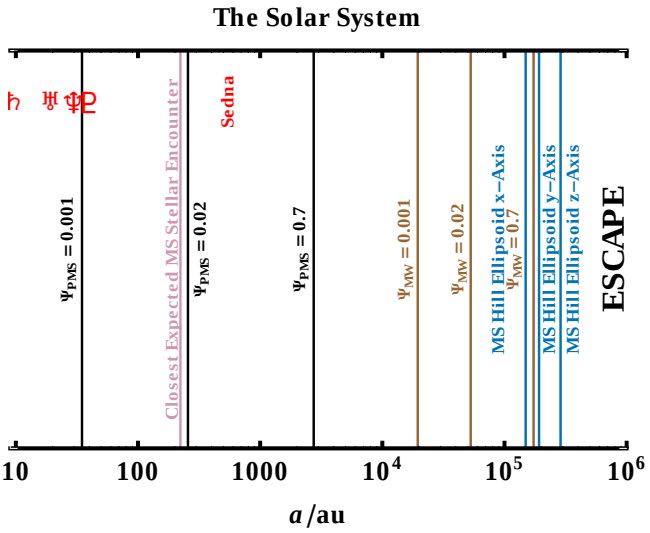

Figure 4. Danger regions of the Solar System. This plot represents a vertical slice of the three plots in Fig. 3, assuming $M_\star = 1M_\odot$ and utilising the same colour scheme. Lines marked $\Psi = 0.001$ correspond to adiabaticity transitions for objects which are sensitive to small changes in orbital behaviour, such as comets with $e \approx 0.99$. Greater values of Ψ indicate higher thresholds for nonadiabatic orbital change. The locations of Saturn, Uranus, Neptune, Pluto (and the Kuiper Belt) and Sedna are marked in red.

4 CHARACTERISTICS OF MOTION

Here, we describe the types of orbital motion which are possible in the different regions partitioned in Fig. 3.

4.1 Orbital elements

Although this motion due to post-MS mass loss and Galactic tides is represented fully by equations (1)-(3), we can glean a much better understanding by converting these equations into orbital elements. The final result is summarized in Table 1. The variables i ω, and Ω represent the inclination, argument of pericentre, and longitude of ascending node of the secondary orbit about the primary with respect to a reference plane which is parallel to and coincident with the Galactic plane. Among the earliest derivations of the full equations of motion due to isotropic stellar mass loss are the studies of Omarov (1962) and Hadjidemetriou (1963). Later Paper I described specific properties of these equations (in column 2 of Table 1), such as the transition from adiabaticity to nonadiabaticity and how the pericentre of the orbit cannot ever decrease due to stellar mass loss alone. The orbital equations due to Galactic perturbations were separately derived for the adiabatic vertical case (in column 3 of Table 1; Brasser 2001), the adiabatic planar case (in part of column 5 of Table 1; Fouchard 2004) and the fully nonadiabatic case (in column 6 of Table 1; Veras & Evans 2013a).

4.2 Escape and collision

The properties of the equations of greatest interest here are the ability of the companion's semimajor axis and eccentricity to expand or shrink. Escape can occur only if $a \to \infty$ and $e \to 1$. If the latter condition holds, but instead the semimajor axis remains finite, then the companion collides with the star. Adiabatic mass loss causes expansion of the orbit but no change in eccentricity, and hence can never cause a companion to escape. Nonadiabatic mass loss also must cause expansion of the orbit, although may cause escape because the eccentricity can be changed (not necessarily increased).

All adiabatic Galactic tides keep a companion's semimajor axis fixed, and hence alone can never cause escape. However, these adiabatic tides continuously cause a change in eccentricity, and hence can create collisions with the parent star. Nonadiabatic Galactic tides can trigger both escape and collision because they may increase or decrease a or e.

4.3 Summary flow chart

Tides act continuously throughout a planet's life and post-MS mass loss of the parent star always occurs, though just for one epoch. In each case at every stage, instability may occur. With these considerations, combined with the properties of motion from Table 1 and the regions of motion in Fig. 3, we create the flowchart Fig. 5.

The flowchart illustrates the possible evolutionary pathways of single-planet systems, from the MS to the WD phase through

Table 1. Equations of motion in terms of orbital elements. The auxiliary set of C_i variables found within the table equations can be expressed in terms of orbital elements by Veras & Evans (2013a).
$C_1 \equiv e\cos\omega + \cos(f+\omega)$, $C_2 \equiv e\sin\omega + \sin(f+\omega)$, $C_3 \equiv \cos i \sin\Omega \sin(f+\omega) - \cos\Omega\cos(f+\omega)$,
$C_4 \equiv \cos i\cos\Omega\sin(f+\omega) + \sin\Omega\cos(f+\omega)$, $C_5 \equiv (3+4e\cos f+\cos 2f)\sin\omega + 2(e+\cos f)\cos\omega\sin f$,
$C_6 \equiv (3+4e\cos f+\cos 2f)\cos\omega - 2(e+\cos f)\sin\omega\sin f$, $C_7 \equiv (3+2e\cos f-\cos 2f)\cos\omega + \sin\omega\sin 2f$, and
$C_8 \equiv (3-\cos 2f)\sin\omega - 2(e+\cos f)\cos\omega\sin f$.

	Mass Loss	Mass Loss	Galactic Tides	Galactic Tides
	Adiabatic	Nonadiabatic	Adiabatic	Nonadiabatic
	Everywhere	Everywhere	Disc Only	Disc Only
$\frac{da}{dt} =$	$-\frac{a}{\mu}\frac{d\mu}{dt}$	$-\frac{a\left(1+e^2+2e\cos f\right)}{1-e^2}\frac{1}{\mu}\frac{d\mu}{dt}$	0	$\frac{2a\sqrt{1-e^2}}{n(1+e\cos f)}C_1\left\{\sin^2 i\sin(f+\omega)\right\}\Upsilon_{zz}$
$\frac{de}{dt} =$	0	$-(e+\cos f)\frac{1}{\mu}\frac{d\mu}{dt}$	$-\frac{5e\sqrt{1-e^2}}{2n}\cos\omega\sin\omega\sin^2 i\Upsilon_{zz}$	$\frac{\left(1-e^2\right)^{\frac{3}{2}}}{2n(1+e\cos f)^2}C_6\left\{\sin^2 i\sin(f+\omega)\right\}\Upsilon_{zz}$
$\frac{di}{dt} =$	0	0	$\frac{5e^2\sin 2\omega\sin 2i}{8n\sqrt{1-e^2}}\Upsilon_{zz}$	$\frac{\left(1-e^2\right)^{\frac{3}{2}}\sin i}{n(1+e\cos f)^2}\left\{\cos i\cos(f+\omega)\sin(f+\omega)\right\}\Upsilon_{zz}$
$\frac{d\Omega}{dt} =$	0	0	$\frac{\cos i\left(2+3e^2-5e^2\cos 2\omega\right)}{4n\sqrt{1-e^2}}\Upsilon_{zz}$	$\frac{\left(1-e^2\right)^{\frac{3}{2}}}{n(1+e\cos f)^2}\left\{\cos i\sin^2(f+\omega)\right\}\Upsilon_{zz}$
$\frac{d\omega}{dt} =$	0	$-\frac{\sin f}{e}\frac{1}{\mu}\frac{d\mu}{dt}$	$\frac{5\sin^2\omega\left(\sin^2 i-e^2\right)-\left(1-e^2\right)}{2n\sqrt{1-e^2}}\Upsilon_{zz}$	$\frac{\left(1-e^2\right)^{\frac{3}{2}}}{2en(1+e\cos f)^2}\left\{-2\sin(f+\omega)\left[e\sin(f+\omega)+\frac{1}{2}C_8\sin^2 i\right]\right\}\Upsilon_{zz}$
$\frac{df}{dt} =$	–	$-\frac{d\omega}{dt}+\frac{n(1+e\cos f)^2}{\left(1-e^2\right)^{3/2}}$	–	$-\frac{d\omega}{dt}-\cos i\frac{d\Omega}{dt}+\frac{n(1+e\cos f)^2}{\left(1-e^2\right)^{3/2}}$

Table 1. Continuation

	Galactic Tides	Galactic Tides
	Adiabatic	Nonadiabatic
	Bulge & Halo	Bulge & Halo
$\frac{da}{dt} =$	0	$\frac{2a\sqrt{1-e^2}}{n(1+e\cos f)}\Big[\Upsilon_{zz}C_1\left\{\sin^2 i\sin(f+\omega)\right\}+\left(\Upsilon_{xx}C_3-\Upsilon_{xy}C_4\right)\left\{C_1\sin\Omega\cos i+C_2\cos\Omega\right\}$ $-\left(\Upsilon_{yx}C_3-\Upsilon_{yy}C_4\right)\left\{C_1\cos\Omega\cos i-C_2\sin\Omega\right\}\Big]$
$\frac{de}{dt} =$	equation (A2) of Veras & Evans (2013b)	$\frac{\left(1-e^2\right)^{\frac{3}{2}}}{2n(1+e\cos f)^2}\Big[\Upsilon_{zz}C_6\left\{\sin^2 i\sin(f+\omega)\right\}+\left(\Upsilon_{xx}C_3-\Upsilon_{xy}C_4\right)\left\{C_6\sin\Omega\cos i+C_5\cos\Omega\right\}-$ $\left(\Upsilon_{yx}C_3-\Upsilon_{yy}C_4\right)\left\{C_6\cos\Omega\cos i-C_5\sin\Omega\right\}\Big]$
$\frac{di}{dt} =$	equation (A3) of Veras & Evans (2013b)	$\frac{\left(1-e^2\right)^{\frac{3}{2}}\sin i}{n(1+e\cos f)^2}\Big[\Upsilon_{zz}\left\{\cos i\cos(f+\omega)\sin(f+\omega)\right\}-\left(\Upsilon_{xx}C_3-\Upsilon_{xy}C_4\right)\left\{\sin\Omega\cos(f+\omega)\right\}$ $+\left(\Upsilon_{yx}C_3-\Upsilon_{yy}C_4\right)\left\{\cos\Omega\cos(f+\omega)\right\}\Big]$
$\frac{d\Omega}{dt} =$	equation (A4) of Veras & Evans (2013b)	$\frac{\left(1-e^2\right)^{\frac{3}{2}}}{n(1+e\cos f)^2}\Big[\Upsilon_{zz}\left\{\cos i\sin^2(f+\omega)\right\}-\left(\Upsilon_{xx}C_3-\Upsilon_{xy}C_4\right)\left\{\sin\Omega\sin(f+\omega)\right\}$ $+\left(\Upsilon_{yx}C_3-\Upsilon_{yy}C_4\right)\left\{\cos\Omega\sin(f+\omega)\right\}\Big]$
$\frac{d\omega}{dt} =$	equation (A5) of Veras & Evans (2013b)	$\frac{\left(1-e^2\right)^{\frac{3}{2}}}{2en(1+e\cos f)^2}\Big[\Upsilon_{zz}\left\{-2\sin(f+\omega)\left[e\sin(f+\omega)+\frac{1}{2}C_8\sin^2 i\right]\right\}$ $-\left(\Upsilon_{xx}C_3-\Upsilon_{xy}C_4\right)\left\{C_8\sin\Omega\cos i-C_7\cos\Omega\right\}+\left(\Upsilon_{yx}C_3-\Upsilon_{yy}C_4\right)\left\{C_8\cos\Omega\cos i+C_7\sin\Omega\right\}\Big]$
$\frac{df}{dt} =$	–	$-\frac{d\omega}{dt}-\cos i\frac{d\Omega}{dt}+\frac{n(1+e\cos f)^2}{\left(1-e^2\right)^{3/2}}$

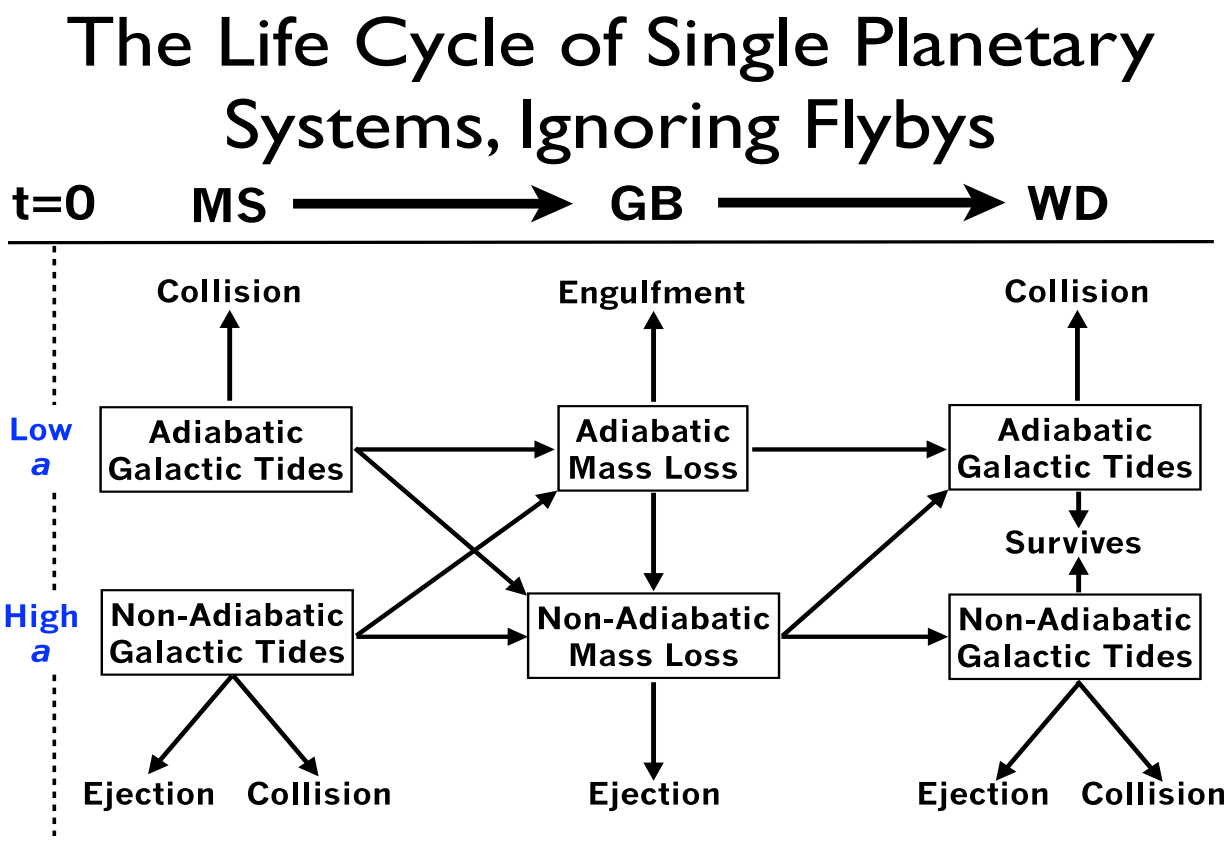

Figure 5. The paths planetary lives tread for parent stars which eventually become white dwarfs (WDs) after a main-sequence (MS) phase and at least one giant branch (GB) phase. This chart assumes that planets are largely unaffected by any close flybys which may occur at any time. By the phrases *low a* and *high a*, we refer to semimajor axes which correspond to points below and above the adiabaticity boundary lines in Fig. 3. For example, for a planet orbiting a $1M_{\odot}$ star in the Solar neighbourhood, the semimajor axis mass loss and Galactic tidal adiabaticity boundaries are at a couple hundred au and several ten thousands of au.

the Giant Branch (GB) phases. All of the mass loss occurs during the GB phases. The chart does not take into account flybys both because of their uncertain occurrence rate and the variety of ways in which they can alter the orbit of a planet or cause instability. However, despite their exclusion, flybys can play important roles in planetary systems, particularly for planets at wide separations.

The instability types listed on the bottom and top rows include

1. "collision": when the planet collides with the star due to Galactic tides. In the adiabatic case, the collision occurs because of an increase in e, whereas in the non-adiabatic case, both a and e are varied.

2. "ejection": when the planet escapes the system. Both non-adiabatic Galactic tides and non-adiabatic mass loss can prompt this action.

3. "engulfment": when stellar tides force a planet to spiral into the expanding envelope.

The chart also relies on the following properties which hold true throughout nearly the entire Milky Way. First, post-MS mass loss during the TPAGB phase is decoupled from Galactic tides because the latter acts on a timescale which is too slow (Fig. 1). Also, adiabatic post-MS mass loss can never expand an orbit in to the nonadiabatic Galactic tidal regime, as also apparent from Fig. 3. Finally, collision with the parent star may always occur due to Galactic tides during the MS or WD phases.

4.4 Fate of adiabatic disc exoplanets

As an application, we consider the evolutionary path that currently-observed Galactic disc exoplanets within tens of au are likely treading. This path corresponds to adiabatic Galactic tidal evolution along the MS, followed by adiabatic AGB mass loss and concludes with adiabatic Galactic tidal evolution along the WD evolution track. The majority of known and candidate planets (see the Extrasolar Planets Encyclopedia at http://exoplanet.eu/, the Exoplanet Data Explorer at http://exoplanets.org/ and the NASA Exoplanet Archive at http://exoplanetarchive.ipac.caltech.edu/) will exhibit this behaviour although roughly half will be destroyed by tidal envelope engulfment during the GB phases. Hence, our heavily-biased exoplanetary system observations fail to cover the full realm of possibilities presented in Fig. 5.

By restricting ourselves to the disc, we can neglect all planar tidal terms (see Veras & Evans 2013b). Further, by restricting ourselves to adiabatic evolution, the relevant equations are in columns 1 and 3 of Table 1. This set of equations does not have a general solution.

However, in special cases, exact solutions do exist for mass loss and Galactic tides separately; for the latter, however, few

results are known. Therefore, a coupled solution is likely to be restricted to extensions of these known results. Thus, we revisit the analytic stationary solutions discussed by Veras & Evans (2013b). In these solutions, the planet is on a permanently polar orbit with $\omega(t) = \omega_0 = \pm\arcsin\left(\sqrt{1/5}\right)$. On this orbit, given enough time, the planet's eccentricity becomes unity, corresponding to instability. Slight deviations from these exact conditions cause substantial perturbations (change of several tenths in eccentricity) over a MS lifetime (about 10 Gyr for a $1M_\odot$ star) for wide-orbit companions (at a few thousand au) in the Galactic disc.

For the purposes of the below computation, assume that mass is being lost at a constant rate such that $\dot{\mu} = G\dot{M}_\star \equiv -\kappa$, where $\kappa > 0$. We attempted to solve the coupled differential equations, now including mass loss, in the same Taylor-expanded manner[4] as Veras & Evans (2013b). However, we obtained no physical solutions. Instead, we found that the exact stationary orbit case ($i = 90^\circ$) does yield solutions, both of which can provide insights into the interplay between mass loss and the Galactic tide. The solutions are:

$$e(t) = \frac{e_0}{\cosh\left[\frac{t\mu_0\Upsilon_{zz}}{n_0(\kappa t-\mu_0)}\right] \mp \sqrt{1-e_0^2}\sinh\left[\frac{t\mu_0\Upsilon_{zz}}{n_0(\kappa t-\mu_0)}\right]}. \quad (36)$$

The eccentricity increases to unity, given enough time. The corresponding survival time is

$$t_{\rm surv} \approx \frac{n_0}{\frac{n_0}{\mu_0}\kappa \mp 2\Upsilon_{zz}\left[\ln\left(\frac{2-e_0^2}{e_0^2} + \frac{2\sqrt{1-e_0^2}}{e_0^2}\right)\right]^{-1}}$$

$$= \frac{1}{n_0\left(\Psi_{\rm PMS}(0) \mp \Psi_{\rm MW}(0)\left[\ln\left(\sqrt{\frac{2-e_0^2}{e_0^2} + \frac{2\sqrt{1-e_0^2}}{e_0^2}}\right)\right]^{-1}\right)}. \quad (37)$$

With the exception of the mass loss term and the additional term in the large radicand, this expression is equivalent to Equation (36) of Veras & Evans (2013b).

The denominator of equation (37) illustrates the interplay between stellar mass loss and Galactic tides. For initially circular orbits, the survival time is dictated entirely by post-MS evolution[5]. As the planet's eccentricity approaches unity, while its semimajor axis is increasing, potential outcomes include colliding with the star or leaving the adiabatic regime. Escape through the Hill sphere, however, is not possible through this mechanism.

To make better sense of this equation, consider a planet in the Solar neighbourhood on a 10^2 yr orbit (adiabatically evolving with mass loss and Galactic tides) around a $2M_\odot$ star such that $n_0 = 2\pi/10^2$yr. From Fig. 1, we have $\Psi_{\rm PMS} < 10^{-3}$ and $\Psi_{\rm MW} \approx 10^{-12}$. The quantity in square brackets is a typically order-of-unity weak function of e_0, varying for example between 0.3 and 3.0 for values of e_0 approximately equal to 0.9565 and 0.0994. Therefore, in this system the mass loss dominates, so in fact $t_{\rm surv} \approx \mu(0)/\dot{\mu}(0)$, which is the time taken for the star to lose all its mass. Because stars that become WDs lose at most about 80 per cent of their mass, $t_{\rm surv}$ is never reached.

As we demonstrate in Fig. 1, for orbital periods corresponding to adiabatic mass loss, $\Psi_{\rm PMS} \gg \Psi_{\rm MW}$ always. For these two terms to be comparable, the logarithmic coefficient of $\Psi_{\rm MW}(0)$ (containing e_0) must be so high that in this case the secondary would collide with the parent star. This example demonstrates that, aside from exceptional circumstances, Galactic tides play a negligible role during post-MS mass loss (as opposed to during MS or WD evolution).

5 DISCUSSION

We now consider the implications of this work on Oort clouds, stellar binary companions and free-floating planets.

5.1 Depletion of Oort clouds after AGB mass loss

MS Oort cloud comets close to the Hill ellipsoid boundary are susceptible to escape during AGB mass loss as the Hill ellipsoid shrinks and the orbit expands. The Hill shrinkage scales as $M_\star^{1/3}$ (equation 21) but the orbital expansion is more complex because of the dependence on eccentricity (column 2 of Table 1). The eccentricity variation prevents us from effectively bounding the nonadiabatic semimajor axis variation except in specific cases (Paper I). A lower bound to the semimajor axis expansion roughly approximates the adiabatic limit[6]. If we use this approximation, then the semimajor axis expansion scales as $M_\star^{-1}$.

We combine these two scalings to produce Fig. 6, in which we plot Oort cloud semimajor axes beyond which the comets must escape on the MS (upper 8 curves) and during post-MS evolution due to mass loss alone (lower 8 curves). Each pair of coloured curves corresponds to a different progenitor stellar mass. The distance between the upper and lower curves in each pair increases for higher stellar masses because those exhibit greater mass loss. Each curve corresponds to the z semiaxis of the Hill ellipsoid, which is always the smallest of the three semiaxes; a comet will not be able to remain bound for an entire orbit if part of that orbit is outside of the Hill ellipsoid.

Flybys, which are not included in this estimate, will still likely play a role in Oort cloud evolution during TPAGB mass loss (Fig. 3). Nevertheless, flybys can keep comets bound only in a fraction of cases. Figure 6 suggests, for example, that for $1M_\odot$ stars in the Solar Neighbourhood, comets beyond about 10^5 au would not remain bound during AGB mass loss. This result corresponds well to fig. 8 of Brasser et al. (2010). Oort clouds in the Galactic bulge are particularly vulnerable to escape. They can remain bound only if they extend inward to semimajor axes under a few thousand au. This limitation suggests that the bulge might be teaming with free-floating comets.

The post-MS danger region is substantial. The fraction of the entire MS Hill ellipsoid that contains the semimajor axis range corresponding to guaranteed mass loss-induced escape is approximately equal to $1 - [1 - M_\star(t_{\rm WD})/M_\star(t_{\rm MS})]^{4/3}$, or 51.5%, 74.7%, 82.7%, 85.3%, 87.3%, 87.8%, 88.3% and 89.0% for progenitor stellar masses of $1M_\odot$, $2M_\odot$, $3M_\odot$, $4M_\odot$, $5M_\odot$, $6M_\odot$, $7M_\odot$, and $8M_\odot$. The location of Oort cloud comets at the onset of post-MS mass loss then crucially determines how

[4] The Taylor expansion is carried out to fourth-order in eccentricity about $e = 0$ and first-order in inclination about $i = 90^\circ$.

[5] One cannot, however, reduce this expression by assuming $\Upsilon_{zz} \to 0$ because in this case $e(t) = e_0$ and $t_{\rm surv}$ has no physical meaning.

[6] For example, Fig. 4 of Paper I helps demonstrate that sub-adiabatic semimajor axis expansion may occur just during the adiabatic transition region. In real systems, this transition region is unlikely to persist for the majority of GB evolution.

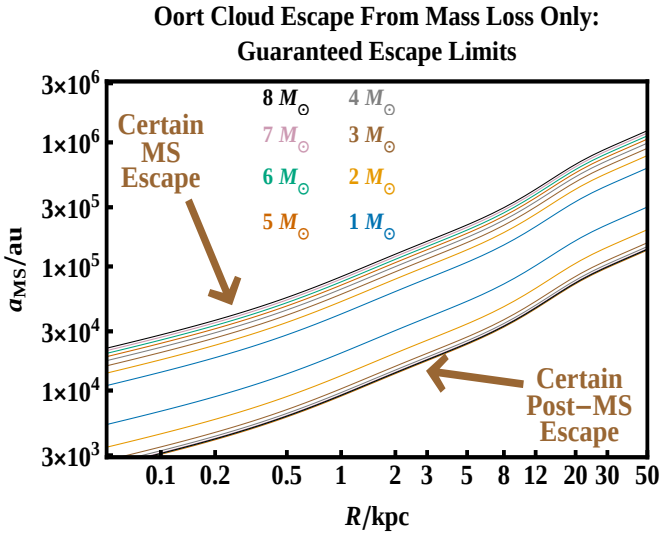

Figure 6. Boundaries beyond which Oort cloud escape definitely occurs on the main-sequence (MS) (upper 8 curves) and during post-MS evolution (lower 8 curves). Each similarly-coloured pair of curves corresponds to a different stellar progenitor mass, which are labeled. In every case, the MS escape boundary is over twice as far away as the post-MS escape boundary. The plot demonstrates that Oort clouds become depleted and excited due to post-MS mass loss.

populated the Milky Way will become with free-floating comets as stars die.

Comets which do remain bound are likely to be highly dynamically excited in eccentricity (e.g. Veras & Wyatt 2012) and inclination. In the latter case, any anisotropy in the mass loss has a pronounced effect in the outer reaches of planetary systems (Parriott & Alcock 1998), and specifically grows in importance as $\sqrt{a}$ and affects the inclination evolution (Veras et al. 2013a). Consequently, the flux of eccentric comets entering the inner WD system might change significantly and could have direct or indirect consequences for explanations of the origin of polluted WD atmospheres (e.g. Zuckerman et al. 2003; Gänsicke et al. 2008; Farihi et al. 2009).

5.2 Two evolving stars

In a binary system with two stars, evolutionary possibilities become significantly more numerous. While both are on the MS, Fig. 3 still applies, except that the nonadiabatic limits are being shifted by order unity due to the secondary mass being of the same order as a Solar mass in equations (19-20). The onset of post-MS evolution can elicit many possible outcomes (Hurley et al. 2002) depending on the stars' masses, metallicities and mutual orbit. If the stars are sufficiently separated from each other that they evolve independently, then the system might undergo two distinct phases of MS evolution before both stars become WDs. If both stars lose mass concurrently, the evolution of the mutual orbit is still dictated by the equations in column 2 of Table 1. Nevertheless, in this case the nonadiabatic limits in Fig. 3 might be shifted more significantly.

We can investigate concurrent stellar evolution in more detail, particularly to determine in what cases the secondary moves off of the MS during post-MS evolution of primary. The most significant coupling of mass loss rates would occur for mass loss on the AGB, and so we consider only that phase. We set primary progenitor masses of $2M_{\odot}$, $3M_{\odot}$, $4M_{\odot}$, $5M_{\odot}$, $6M_{\odot}$, $7M_{\odot}$ and $8M_{\odot}$, and assume the primaries and secondaries are born at the same time, evolve independently, and initially contain Solar metallicity. We then use `SSE` to trace the evolution of lower-mass secondaries, in decrements of $0.02M_{\odot}$ from the initial primary mass, until the total mass loss of the system is always dictated by just one of the stars. All simulations make the same assumptions about mass loss as in the rest of the paper. By using `SSE` rather than the binary version, `BSE` (Hurley et al. 2002), we avoid introducing many additional parameters which are unnecessary for this basic exploration.

We find that in nearly every case, the secondary mass must be within 10 per cent of the progenitor primary mass in order to achieve mass loss coupling during their AGB phases. Specifically, we find that the highest secondary progenitor masses that demonstrate decoupling are $1.82, 2.74, 3.70, 4.68, 5.62, 6.56, 7.16M_{\odot}$. The probability that a binary pair is so closely matched in mass varies as a function of stellar type. O-type binaries typically feature nearly equal-mass stars (Zinnecker & Yorke 2007) whereas less massive stars demonstrate a greater range of mass ratios (e.g. Metchev & Hillenbrand 2009). In this scenario, mass loss coupling amongst the highest mass binaries will have the greatest consequences for shifting the nonadiabatic limits in Fig. 3. However, recent work claiming that the mass ratio distribution is essentially flat for all primaries more massive than $0.3M_{\odot}$ (Duchêne & Kraus 2013) demonstrates that perhaps the coupling probability is largely independent of total system mass.

A planet may be introduced in this system orbiting one of the stars (circumstellar) or orbiting both stars (circumbinary). Tens of percent of all confirmed exoplanets reside in binary systems. Most of these planets orbit in a circumstellar manner. However, recent circumbinary exoplanet discoveries (Doyle et al. 2011; Orosz et al. 2012a,b; Welsh et al. 2012) have helped incite interest in multiple stellar-component planetary systems.

We do not fully calculate systems with a third body but we can provide a rough estimate of the consequences. The circumbinary case may be reduced to a 2-body system if the binary separation is much less than the distance to the orbiting planet. In paper II we demonstrated that, in this case, the key quantity to determine the orbital evolution is the overall mass-loss rate from the binary system. Paper II also showcased how this rate is a complex function of the phase space. Applied to our Fig. 3, the position of each black horizontal line would be a function of the properties of both stars. The other figure curves would remain largely unchanged. In paper II we demonstrated that circumbinary systems feature, generally, much smaller mass-loss adiabaticity boundaries than for the single-star case. Consequently, the potential evolutionary pathways in Fig. 5 would remain unchanged.

For circumstellar orbits in binary systems, planetary motion can no longer be modelled with Figs. 3 and 5. Even without any mass loss, planets may bounce between binary stars on the MS (Moeckel & Veras 2012). Post-MS evolution can then cause an exchange reaction allowing a planet to hop from the evolving star to the non-evolving companion, around which the planet can attain a stable orbit (Kratter & Perets 2012). How Galactic tides and stellar flybys alter these and similar situations represents an interesting topic for future investigation.

5.3 Free-floating bodies

This work's emphasis on escape motivates discussion of the Milky Way's population of substellar-mass objects which are not gravitationally bound to a single or small group of stars. These bodies have been referred to in the literature by several terms, including free-floating planets and cluster planets (see e.g. the Extrasolar Planet Encyclopedia at http://exoplanet.eu/), rogue planets, sub brown-dwarfs (e.g. Pg. 7 of Perryman 2011), nomads (e.g. Strigari et al. 2012) and isolated planetary-mass objects (e.g. Delorme et al. 2012). The ambiguity arises from both the uncertain deuterium-burning mass limit (see e.g. Spiegel et al. 2011) and the multiple potential formation pathways for these objects.

Observations of free-floaters have been plagued by uncertain mass determinations that arise from a degeneracy between the luminosity, mass and age of the objects. This uncertainty has placed doubt as to whether any of these objects are below the deuterium-burning mass limit, despite the mass errors quoted (see the Extrasolar Planet Encyclopedia). Recently, this degeneracy has finally been broken: Delorme et al. (2012) has discovered and associated the $4M_J$-$7M_J$ T-type exoplanet CFBDSIRJ214947.2-040308.9 with the AB Doradus moving group with an 87% probability. Membership helps ensure that this free-floater is of planetary-mass and ultimately that free-floating planets do exist.

This near-confirmation, as well as the astonishing estimate that the Milky Way's free-floating giant planet population exceeds the bound giant planet population (Sumi et al. 2011), motivates determination of the free-floating planet formation pathways. Although molecular cloud collapse triggers star formation, the resulting fragmentation may also produce planetary-mass objects which become free-floating. Alternatively, free-floating planets may have been originally formed from protoplanetary disc fragmentation, and only later in life have escaped due to instability within the system. Many candidate free-floating planets have been discovered in young, star-forming clusters (see references on Pg. 215 of Perryman 2011) and in the field (see references in Delorme et al. 2012), thereby largely failing to constrain the dominant formation pathway. Free-floaters formed by cloud fragmentation could later appear isolated in the field, and free-floaters formed by disc fragmentation could be stripped off of their parent stars in both clusters (Adams et al. 2006; Fregeau et al. 2006; Spurzem et al. 2009; Malmberg et al. 2011; Boley et al. 2012; Parker & Quanz 2012) and in the field (Zakamska & Tremaine 2004; Varvoglis et al. 2012; Veras & Moeckel 2012). Additional sources include ejection from planet-planet scattering (e.g. Veras & Raymond 2012) and post-main sequence instability (Paper I; Paper II; Adams et al. 2013; Mustill et al. 2013a,b; Veras et al. 2013b; Voyatzis et al. 2013).

Our work suggests that if a population of planets exist on the MS at distances corresponding to $a \gg 100$ au, then the combined effects of post-MS mass loss, Galactic tides and flybys yields a free-floating planet population that may be strongly dependent on age and Galactic location. The oldest regions of the bulge would feature the highest sub-populations, and the youngest regions of the halo the lowest. The overall population is unlikely to scale strongly with stellar mass, because the adiabatic mass loss limits in all three plots of Fig. 3 are well-separated from the adiabatic Galactic tidal limit. Only beyond this limit is escape possible (see columns 3-6 of Table 1) after a planet survives post-MS evolution and withstands the effects of stellar flybys. The distribution of Oort cloud comets in the interstellar medium is similarly dependent on age and location. However, these objects are not yet detectable. The forthcoming all-sky survey missions GAIA and LSST will be able to detect free-floaters which have masses that exceed about 1 M_J, whereas WFIRST will be able to probe the population of free-floaters at lower masses (Strigari et al. 2012).

6 CONCLUSION

We have identified when and where planetary, cometary and binary systems are most affected by the collusion of three important perturbations, post-MS mass loss, Galactic tides and stellar flybys. Two of these forces are external, and one internal; two of these must occur, whereas one may occur. By considering the entire range of WD progenitor stars in the Galactic bulge, disc and halo with all possible primary-secondary separations (Fig. 3), we obtain a representative picture of the possible evolutionary pathways and potential instabilities experienced by a stellar system with a single substellar companion (Fig. 5).

Despite a complete analytical characterization of the orbital changes induced by two of these effects (Table 1), the unknown prevalence and orientation of stellar flybys, and their open-ended consequences (Section 3.5.4) prevent us from establishing conclusions more specific than the ones listed below. An outstanding feature of nearly all these conclusions is their applicability throughout the Milky Way.

1. **Everywhere in Galaxy:** AGB mass loss is decoupled from Galactic tides (Fig. 1): the former dominates over the duration of the mass loss. Also, barring exceptional circumstances, AGB mass loss will run its course without disruption from close stellar flybys if the secondary is close enough to the primary such that the mass loss is adiabatic.

2. **Everywhere in Galaxy:** Adiabatic mass loss cannot by itself expand the secondary's orbit into the nonadiabatic Galactic region.

3. **Everywhere in Galaxy:** Adiabatic Galactic tidal effects cannot cause escape and the smallest Hill axis is always a factor of about $(2/\Psi_{\rm MW})^{3/4} \approx 2-300$ beyond the nonadiabatic Galactic boundary. Hence, if a secondary survives AGB mass loss but fails to reach this boundary, the body can escape the WD only through flybys.

4. **Everywhere in Galaxy:** The combined effects of Hill ellipsoid shrinkage and secondary orbital excitement due to AGB mass loss (Fig. 6) are likely to decimate a bound MS Oort cloud population and alter the cometary flux into the inner WD system.

5. **Everywhere in Galaxy:** The evolution of binary stars can also be approximated as in Figs. 3 and 5 unless they are close enough to each other to tidally interact, and only if they leave the MS at different times.

6. **In bulge only:** All types of secondaries except for hot Jupiters or similarly-tight binary companions endure strong perturbations from close flybys. Consequently, we expect the frequency of ejections, and generally the amount of free-floating material, to be significantly more abundant in the bulge than in the disc or halo.

ACKNOWLEDGMENTS

We thank the referee for useful comments that have improved the quality of this manuscript. This work benefited from support by the European Union through ERC grant numbers 279973 and 320964. CAT thanks Churchill College for his fellowship.

REFERENCES

Adams, F. C., Anderson, K. R., & Bloch, A. M. 2013, MNRAS, 432, 438
Adams, F. C., & Bloch, A. M. 2013, Submitted to ApJL
Adams, F. C., Proszkow, E. M., Fatuzzo, M., & Myers, P. C. 2006, ApJ, 641, 504
Bear, E., Soker, N., & Harpaz, A. 2011, ApJL, 733, L44
Bear, E., & Soker, N. 2012, ApJL, 749, L14
Binney, J. J., & Evans, N. W. 2001, MNRAS, 327, L27
Binney, J., & Tremaine, S. 2008, Galactic Dynamics: Second Edition, Princeton University Press, Princeton
Boley, A. C., Payne, M. J., & Ford, E. B. 2012, ApJ, 754, 57
Bonnell, I. A., Smith, K. W., Davies, M. B., & Horne, K. 2001, MNRAS, 322, 859
Bonsor, A., Mustill, A. J., & Wyatt, M. C. 2011, MNRAS, 414, 930
Bonsor, A., & Wyatt, M. 2010, MNRAS, 409, 1631
Bottema, R. 1993, AA, 275, 16
Brasser, R. 2001, MNRAS, 324, 1109
Brasser, R., Higuchi, A., & Kaib, N. 2010, A&A, 516, A72
Brasser, R., & Morbidelli, A. 2013, Icarus, 225, 40
Carlberg, J. K., Majewski, S. R., & Arras, P. 2009, ApJ, 700, 832
Collins, B. F., & Sari, R. 2010, AJ, 140, 1306
de Juan Ovelar, M., Kruijssen, J. M. D., Bressert, E., et al. 2012, A&A, 546, L1
Debes, J. H., & Sigurdsson, S. 2002, ApJ, 572, 556
Debes, J. H., Walsh, K. J., & Stark, C. 2012, ApJ, 747, 148
Delorme, P., Gagné, J., Malo, L., et al. 2012, A&A, 548, A26
Doyle, L. R., Carter, J. A., Fabrycky, D. C., et al. 2011, Science, 333, 1602
Duchêne, G., & Kraus, A. 2013, ARA&A, 51, 269
Duncan, M., Quinn, T., & Tremaine, S. 1987, AJ, 94, 1330
Dybczyński, P. A. 2006, A&A, 449, 1233
Emel'Yanenko, V. V., Asher, D. J., & Bailey, M. E. 2007, MNRAS, 381, 779
Evans, N. W. 1993, MNRAS, 260, 191
Evans, N. W., & Collett, J. L. 1993, MNRAS, 264, 353
Farihi, J., Jura, M., & Zuckerman, B. 2009, ApJ, 694, 805
Fouchard, M. 2004, MNRAS, 349, 347
Fouchard, M., Froeschlé, C., Valsecchi, G., & Rickman, H. 2006, Celestial Mechanics and Dynamical Astronomy, 95, 299
Fregeau, J. M., Chatterjee, S., & Rasio, F. A. 2006, ApJ, 640, 1086
Gänsicke, B. T., Koester, D., Marsh, T. R., Rebassa-Mansergas, A., & Southworth, J. 2008, MNRAS, 391, L103
Hadjidemetriou, J. D. 1963, Icarus, 2, 440
Heggie, D. C. 1975, MNRAS, 173, 729
Heggie, D. C., & Rasio, F. A. 1996, MNRAS, 282, 1064
Heisler, J., & Tremaine, S. 1986, Icarus, 65, 13
Hernquist, L. 1990, ApJ, 356, 359
Hills, J. G. 1984a, AJ, 89, 1559
Hills, J. G. 1984b, Nature, 311, 636
Hills, J. G. 1984c, AJ, 89, 1811
Hills, J. G., & Fullerton, L. W. 1980, AJ, 85, 1281
Hills, J. G. 1986, The Galaxy and the Solar System, 397
Hurley, J. R., Pols, O. R., & Tout, C. A. 2000, MNRAS, 315, 543
Hurley, J. R., Tout, C. A., & Pols, O. R. 2002, MNRAS, 329, 897
Jiang, Y.-F., & Tremaine, S. 2010, MNRAS, 401, 977
Jiménez-Torres, J. J., Pichardo, B., Lake, G., & Throop, H. 2011, MNRAS, 418, 1272
Jiménez-Torres, J. J., Pichardo, B., Lake, G., & Segura, A. 2013, Astrobiology, 13, 491
Kaib, N. A., & Quinn, T. 2009, Science, 325, 1234
Kaib, N. A., Raymond, S. N., & Duncan, M. 2013, Nature, 493, 381
Kormendy, J., & Kennicutt, R. C., Jr. 2004, ARAA, 42, 603
Kratter, K. M., & Perets, H. B. 2012, ApJ, 753, 91
Kunitomo, M., Ikoma, M., Sato, B., Katsuta, Y., & Ida, S. 2011, ApJ, 737, 66
Laughlin, G., & Adams, F. C. 1998, ApJL, 508, L171
Malmberg, D., de Angeli, F., Davies, M. B., et al. 2007, MNRAS, 378, 1207
Malmberg, D., Davies, M. B., & Heggie, D. C. 2011, MNRAS, 411, 859
Marzari, F., & Picogna, G. 2013, A&A, 550, A64
Matese, J. J., & Whitmire, D. 1996, ApJL, 472, L41
Maxted, P. F. L., Napiwotzki, R., Dobbie, P. D., & Burleigh, M. R. 2006, Nature, 442, 543
Metchev, S. A., & Hillenbrand, L. A. 2009, ApJS, 181, 62
Moeckel, N., & Veras, D. 2012, MNRAS, 422, 831
Mustill, A. J., & Villaver, E. 2012, ApJ, 761, 121
Mustill, A. J., Veras, D., & Villaver, E. 2013a, Submitted to MNRAS
Mustill, A. J., Marshall, J. P., Villaver, E., Veras, D., Davis, P. J., Horner, J. & Wittenmyer, R.A. 2013b, In Press, MNRAS, arXiv:1309.3881
Nordhaus, J., Spiegel, D. S., Ibgui, L., Goodman, J., & Burrows, A. 2010, MNRAS, 408, 631
Nordhaus, J., & Spiegel, D. S. 2013, MNRAS, 432, 500
Omarov, T. B. 1962, Izv. Astrofiz. Inst. Acad. Nauk. KazSSR, 14, 66
Orosz, J. A., Welsh, W. F., Carter, J. A., et al. 2012a, Science, 337, 1511
Orosz, J. A., Welsh, W. F., Carter, J. A., et al. 2012b, ApJ, 758, 87
Parravano, A., McKee, C. F., & Hollenbach, D. J. 2011, ApJ, 726, 27
Parker, R. J., & Goodwin, S. P. 2009, MNRAS, 397, 1041
Parker, R. J., & Quanz, S. P. 2012, MNRAS, 419, 2448
Parriott, J., & Alcock, C. 1998, ApJ, 501, 357
Passy, J.-C., Mac Low, M.-M., & De Marco, O. 2012, ApJL, 759, L30
Parriott, J., & Alcock, C. 1998, ApJ, 501, 357
Perets, H. B., & Kouwenhoven, M. B. N. 2012, ApJ, 750, 83
Perryman, M. 2011, The Exoplanet Handbook by Michael Perryman, Cambridge University Press; 1 edition, 424 p., ISBN: 0521765595,
Portegies Zwart, S. 2013, MNRAS, 429, L45
Rickman, H., Fouchard, M., Froeschlé, C., & Valsecchi, G. B. 2008, Celestial Mechanics and Dynamical Astronomy, 102, 111
Rickman, H. 2013, Meteoritics and Planetary Science, 302

Singh, J. 2011, AP&SS, 333, 61
Smith, K. W., & Bonnell, I. A. 2001, MNRAS, 322, L1
Soker, N. 1998, AJ, 116, 1308
Spiegel, D. S., Burrows, A., & Milsom, J. A. 2011, ApJ, 727, 57
Spiegel, D. S. 2012, arXiv:1208.2276
Spurzem, R., Giersz, M., Heggie, D. C., & Lin, D. N. C. 2009, ApJ, 697, 458
Strigari, L. E., Barnabè, M., Marshall, P. J., & Blandford, R. D. 2012, MNRAS, 423, 1856
Sumi, T., Kamiya, K., Bennett, D. P., et al. 2011, Nature, 473, 349
Thies, I., Kroupa, P., Goodwin, S. P., Stamatellos, D., & Whitworth, A. P. 2011, MNRAS, 417, 1817
Thompson, T. A. 2013, MNRAS, 883
Valtonen, M., & Karttunen, H. 2006, The Three-Body Problem, by Mauri Valtonen and Hannu Karttunen, ISBN 0521852242. Cambridge, UK: Cambridge University Press, 2006.
van der Kruit, P. C., & Freeman, K. C. 2011, ARAA, 49, 301
Varvoglis, H., & Hadjidemetriou, J. D. 2012, Ap&SS, 339, 207
Varvoglis, H., Sgardeli, V., & Tsiganis, K. 2012, Celestial Mechanics and Dynamical Astronomy, 113, 387
Vassiliadis, E., & Wood, P. R. 1993, ApJ, 413, 641
Veras, D., & Evans, N.W. 2013a, Celestial Mechanics and Dynamical Astronomy, 115, 123
Veras, D., & Evans, N. W. 2013b, MNRAS, 430, 403
Veras, D., Hadjidemetriou, J. D., Tout, C. A. 2013a, In Press, MNRAS, arXiv:1308.0599
Veras, D., & Moeckel, N. 2012, MNRAS, 425, 680
Veras, D., Mustill, A. J., Bonsor, A., & Wyatt, M. C. 2013b, MNRAS, 431, 1686
Veras, D., & Raymond, S. N. 2012, MNRAS, 421, L117
Veras, D., & Tout, C. A. 2012, MNRAS, 422, 1648
Veras, D., & Wyatt, M. C. 2012, MNRAS, 421, 2969
Veras, D., Wyatt, M. C., Mustill, A. J., Bonsor, A., & Eldridge, J. J. 2011, MNRAS, 1332
Villaver, E. 2011, American Institute of Physics Conference Series, 1331, 21
Villaver, E., & Livio, M. 2007, ApJ, 661, 1192
Villaver, E., & Livio, M. 2009, ApJL, 705, L81
Voyatzis, G., Hadjidemetriou, J. D., Veras, D., & Varvoglis, H. 2013, MNRAS, 769
Welsh, W. F., Orosz, J. A., Carter, J. A., et al. 2012, Nature, 481, 475
Wilkinson, M. I., Evans, N. W., 1999, MNRAS, 310, 645
Zakamska, N. L., & Tremaine, S. 2004, AJ, 128, 869
Zhang, M.-J. 2012, AP&SS, 340, 209
Zinnecker, H., & Yorke, H. W. 2007, ARA&A, 45, 481
Zuckerman, B., Koester, D., Reid, I. N., Hünsch, M. 2003, ApJ, 596, 477